CORA Cork Open Research Archive
Cartlann Taighde Oscailte Chorcaí

Title	A novel RCS based CRFID tag design
Authors	Rather, Nadeem;Buckley, John;O'Flynn, Brendan;Pigeon, Melusine
Publication date	2022-05-11
Original Citation	Rather, N., Buckley, J., O'Flynn, B. and Pigeon, M. (2022) 'A novel RCS based CRFID tag design' 2022 16th European Conference on Antennas and Propagation (EuCAP), Madrid, Spain, 27 March-1 April, pp. 1-5. doi: 10.23919/EuCAP53622.2022.9769588.
Type of publication	Conference item
Link to publisher's version	10.23919/EuCAP53622.2022.9769588
Rights	© 2022, IEEE. Personal use of this material is permitted. Permission from IEEE must be obtained for all other uses, in any current or future media, including reprinting/republishing this material for advertising or promotional purposes, creating new collective works, for resale or redistribution to servers or lists, or reuse of any copyrighted component of this work in other works.
Download date	2026-11-08 10:25:39
Item downloaded from	https://hdl.handle.net/10468/12601

UCC
University College Cork, Ireland
Coláiste na hOllscoile Corcaigh

A Novel RCS based CRFID Tag Design

Nadeem Rather[1], John Buckley, Brendan O'Flynn, Melusine Pigeon
Wireless Sensor Network group, Tyndall National Institute, University College Cork, Cork, Ireland, [1] nadeem.rather@tyndall.ie

***Abstract*—In this paper, a Chipless RFID tag design based on Radar Cross Section (RCS) operating principle is proposed. The tag is implemented using a series of circular ring resonators to enable tag identification. The resonators are simulated and then fabricated on an FR4 substrate. A calibration technique using a ring resonator to improve the detection of 8-bit data is proposed and demonstrated. The fabricated tag is measured at a distance of 160 mm using the monostatic RCS method. The measurement results verify the simulation results and show accurate detection of the encoded information.**

***Index Terms*—antennas, chipless RFID, circular ring resonators, measurements, radar cross section.**

I. INTRODUCTION

Chipless Radio Frequency Identification (CRFID) technology is a low-cost passive RFID solution (Less than a cent per tag) as it does not require an RFID chip to operate [1, 2]. Compared to passive chip-based RFID, which utilizes an RFID chip to store a variety of information (Such as Identification and Sensing data [3]) and modulate the signal, CRFID uses the antenna structure to encode identification information [4]. In chipped RFID, a sensor can be integrated with the chip to sense a parameter, such as temperature [5]. In CRFID, an antenna element such as a resonator can be used as a sensor. The identification and sensing information can be encoded in the structural mode of the antenna and retrieved using a specific operating principle [4]. The CRFID operates based on time domain, frequency (spectral) domain, and hybrid methods [6].

In this paper, an 8-bit CRFID tag with novel calibration ring principle is designed, simulated and verified by measurements. The operating principle is based on Radar Cross Section (RCS) measurement of the tag, one of the frequency domain operating principles [7-15]. The RCS is measured using the on-off keying (OOK) amplitude modulation method in chipped RFID tags [2]. However, to perform OOK in CRFID the presence and absence of the resonators is utilized to vary RCS magnitude along the frequency band in the RCS response. The variations can also be achieved by detuning the resonators by short-circuiting or open-circuiting them. The OOK modulation in chipped RFID is performed in the time domain, whereas in CRFID that is performed in the frequency domain [2].

The RCS of a CRFID tag is measured to retrieve the backscattered electromagnetic (EM) signature. The measured RCS response contains the maxima and minima used for encoding bit information [6]. The specific RCS response is achieved by using resonators of different resonant frequencies [16]. When an EM wave is incident towards the target (Tag), it reflects the overall RCS along the frequency band (Shown in Fig.1).

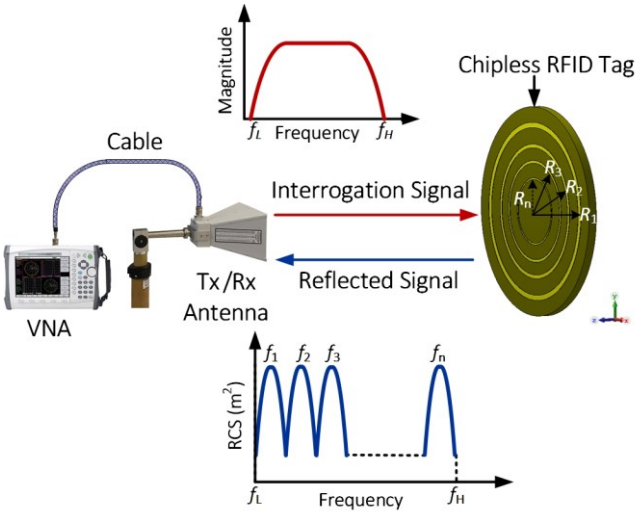


Fig. 1. Overview of the RCS based Chipless RFID operating principle.

The resonators are excited by the transmitted EM wave at specific frequencies and reflected. The reflected wave creates maxima and minima in the RCS response seen by the receiver antenna. The sequential maxima and minima can thus be used to represent the bits. The change in resonance (Magnitude or Phase) to change in the resonator could be used for sensing [17, 18]. RCS of the tag is a function of; Polarization of the incident wave, angle of incidence and reflection, the structural geometry and electrical properties of the tag, and the frequency of operation. It is measured in units of square meters (m^2) or in decibels as $dB(m^2)$ or dBsm [2].

A single layer CRFID tag (without a ground plane) is developed and measured using a single linearly polarized antenna for monostatic RCS detection [19]. The ultra-wide frequency band (UWB) of 3.1 to 10.6 GHz is used to encode the identification information, as discussed in the literature [20]. This paper is divided further into four sections. Section II discusses the key innovation of using a calibration bit principle in the tag design. Section III analyses the results from simulation and measurements for verification, Section IV compares the work with state of the art and, Section V concludes this paper with some discussion and future work.

II. CRFID TAG DESIGN

A. Chipless Tag design principles

The CRFID tag is designed using microstrip Circular Ring Resonators (CRR) [21], as shown in Fig. 2. A total of ten rings on a 25 mm diameter FR4 disk are proposed for this design. The CRR are advantageous in terms of being insensitive to the polarization angle of the incident wave[14].

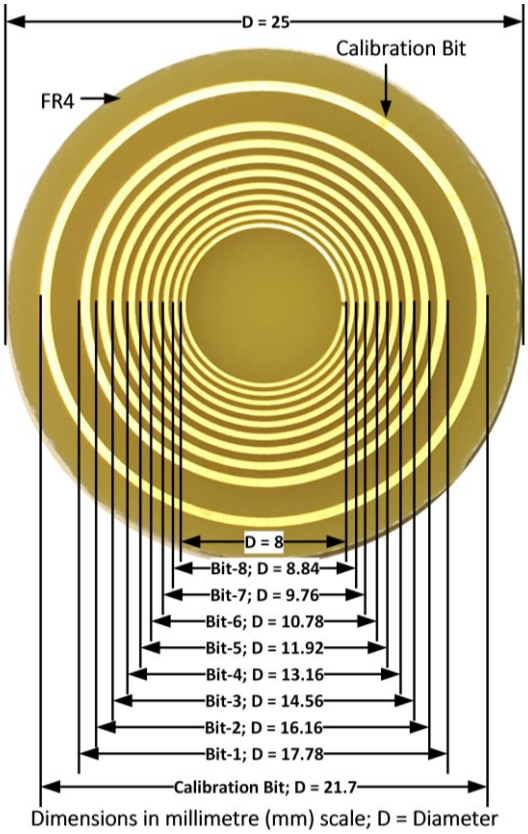


Fig. 2. Final prototype of an 8-bit CRFID tag.

In our design, the outermost CRR is used as a calibration ring. The next eight rings are used for 8-bit data encoding. These will be discussed in detail in the following subsection. The innermost split-ring resonator is reserved for future work to test the sensing capability of the tag. Moreover, it can be used as the ninth bit for identification tags. The information from the tag is retrieved by measuring its RCS. CST microwave studio software [22] is used to simulate the tag. A vertically polarized plane wave is used to remotely excite the tag, and an RCS probe is used for measuring the RCS of the CRFID tag. The 1 mm thick FR4 substrate (Permittivity (ε_r) = 4.6 and Tan δ = 0.025) is used with resonators made of copper of 0.035 mm thickness. In free space, the perimeter of a closed circular ring resonator is approximately equal to the resonant wavelength (λ) of the ring [16]. A nested ring configuration is used in the final design, which utilizes the area within a CRR to improve bit capacity without increasing the tag size. However, when the resonator rings are close, mutual coupling occurs, affecting their resonant frequencies and radiating properties. The mutual coupling effect is difficult to model [14]. To predict the resonance frequency of each ring based on its perimeter, the mutual coupling between the rings is reduced as much as possible without increasing tag size.

B. Encoding and Calibration ring principle

In this paper, the RCS minima are used to represent the bit '1' and a missing ring and the absence of its minima to represent bit '0'[2].

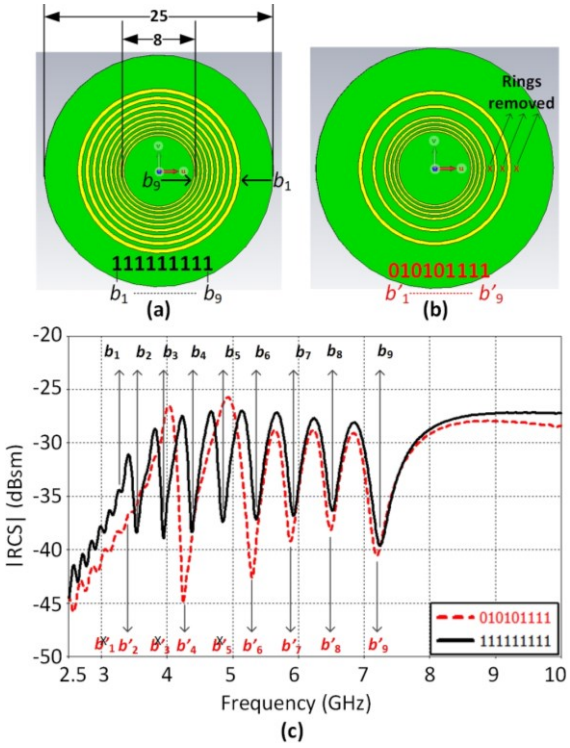


Fig. 3. Encoding principle of 9-bit CRFID tag without calibration bit, (a) 111111111 tag, (b) 010101111 tag, and (c) Simulated RCS response.

A 9-bit CRFID tag is simulated with all rings present to encode '111111111'. The innermost ring is used for encoding to verify encoding and calibration ring principle. As shown in Fig.3a, all the nine rings (b_1 to b_9) are simulated and their RCS response are shown in Fig.3c. This "all 1" encoding will be taken as a reference to show the relevance of addition of the calibration ring in the design. A different bit combination (010101111) is encoded by removing the bit '0' related rings (b_1, b_3, and b_5) (Fig.3b). It is found that when the rings are removed the minima associated with it (b'_1, b'_3, and b'_5) are also removed from the RCS response, however, the minima (b'_2, b'_4, b'_6, b'_7, b'_8, and b'_9) of the bit '1' related rings shifts in frequency compared to the all '1' encoded tag. For decoding a different bit combination, the shift in minima positions would introduce errors in data processing. The errors in this case are gathered in the first column of Table I. Therefore, a novel approach with a calibration ring is proposed, as shown in Fig.4.

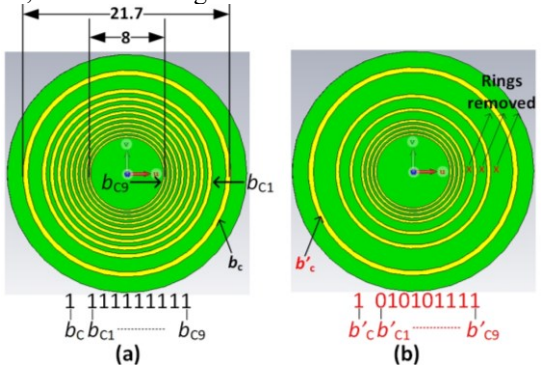


Fig. 4. Tag design with calibration ring (a) 111111111 (b) 010101111.

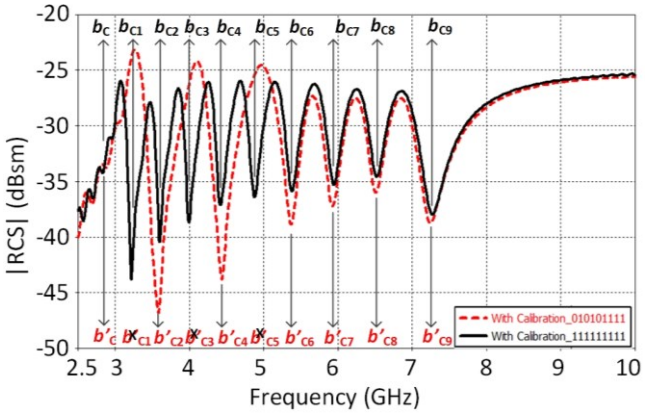


Fig. 5. Simulated RCS response of 111111111 and 010101111 with calibration ring.

The calibration ring creates a minimum (b_c) in the RCS response, which supports the decoding of different bit combinations efficiently. In Fig.4a, the bit combination (111111111) employing the calibration bit principle is simulated. The minima (b_{C1} to b_{C9}) represent the encoded data accurately for '111111111'. Further, when the rings (b_{C1}, b_{C3}, and b_{C5}) are removed to encode (010101111), shown in Fig.4b, the corresponding minima (b'_{C1}, b'_{C3}, and b'_{C5}) are removed. The simulated RCS response is shown in Fig.5. The percentage error between the expected positions of the minima in the frequency band to the observed positions are gathered in Table I and are calculated using equation 1. Such that, the observed value corresponds to b'_2, b'_4, b'_6, b'_7, b'_8, and b'_9 and reference values to b_2, b_4, b_6, b_7, b_8, and b_9 for the case without calibration. Similarly, the percentage error for the RCS response for the case with calibration ring is calculated by using observed values (b'_{C2}, b'_{C4}, b'_{C6}, b'_{C7}, b'_{C8}, and b'_{C9}) and reference values (b_{C2}, b_{C4}, b_{C6}, b_{C7}, b_{C8}, and b_{C9}).

$$\% \text{ Error} = \frac{\text{Observed value} - \text{True Value}}{\text{True Value}} \times 100\ \% \qquad (1)$$

TABLE I Percentage error comparison of with and without calibration ring principle.

Without Calibration		**With Calibration**	
Bit encoding **(010101111)**	**% Error**	Bit encoding **(010101111)**	**% Error**
b'_1 (0)	-	b'_{C1} (0)	-
b'_2 (1)	-5.7	b'_{C2} (1)	-0.38
b'_3 (0)	-	b'_{C3} (0)	-
b'_4 (1)	-2.7	b'_{C4} (1)	-0.33
b'_5 (0)	-	b'_{C5} (0)	-
b'_6 (1)	-1.16	b'_{C6} (1)	-0.12
b'_7 (1)	-1.01	b'_{C7} (1)	-0.21
b'_8 (1)	-0.74	b'_{C8} (1)	-0.17
b'_9 (1)	-1.1	b'_{C9} (1)	-0.27

The calibration ring principle reduces the errors significantly from an average error of -2.06% (without calibration) to -0.27% (with calibration), which is 86.9% percentage error reduction. The reduction in error improves the decoding efficiency. This method provides an efficient 9-bit CRFID tag design, which can be used to encode and decode information with accurate results.

III. MEASUREMENTS

The final prototype of the 8-bit CRFID tag with calibration ring and a reserved sensing bit is fabricated for three different bit combinations. In terms of the RCS magnitude of the tag and available resonators to reflect EM waves, a best-case Tag-1 (11111111), a worst-case Tag-2 (00000001), and a random test-case Tag-3 (00011100) for our measurements are chosen, as shown in Fig. 6. The split gap in the innermost ring is short-circuited by a 0.1 pF capacitor (04/02 package) to verify our 8-bit encoding results.

A. Measurement procedure

RCS measurements can be carried out using bi-static or monostatic measurement methods [19]. A vector network analyzer (VNA) is used to measure RCS from the transmission and reflection coefficients [23].

In this paper, the monostatic approach using a single linearly polarized horn antenna (Schwarzbeck BBHA9120D) is used for transmission and reception of EM waves. It reduces the overall measurement complexity. A calibration method derived from [23], is used to calculate the RCS from reflection coefficients (Equation 2).

$$\text{RCS}\ (\sigma) = \left|\frac{S_{11_{Tag}} - S_{11_{Iso}}}{S_{11_{Ref}} - S_{11_{Iso}}}\right|^2 \times \sigma_{Ref} \quad \text{m}^2 \qquad (2)$$

An Anritsu MS2038C VNA [24] is used to generate a frequency sweep of 3.1 to 10.6 GHz (0 dBm output power) and record one port reflection coefficient (S_{11}). The tag is placed on a EM transparent structure at a distance of 160 mm from the horn antenna (Fig.7). The measurements are carried out in a closed laboratory room with RF absorbers placed behind the tag to reduce unwanted signal reflections from the surrounding environment in the measurement.

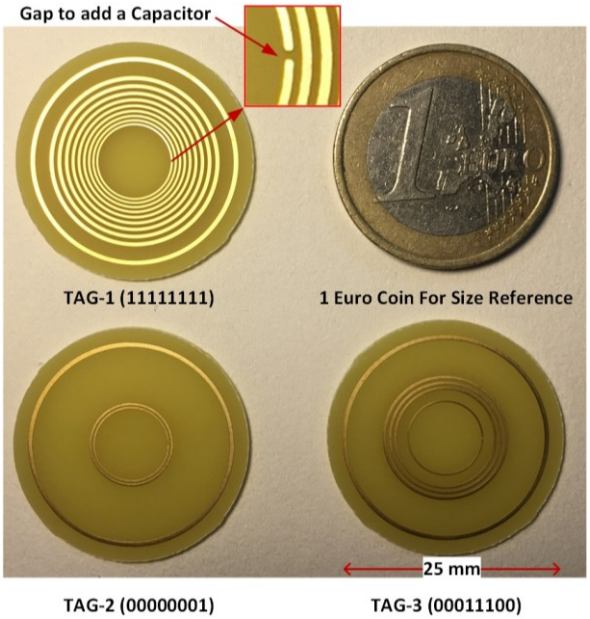


Fig. 6. Fabricated CRFID tags for verification by measurements.

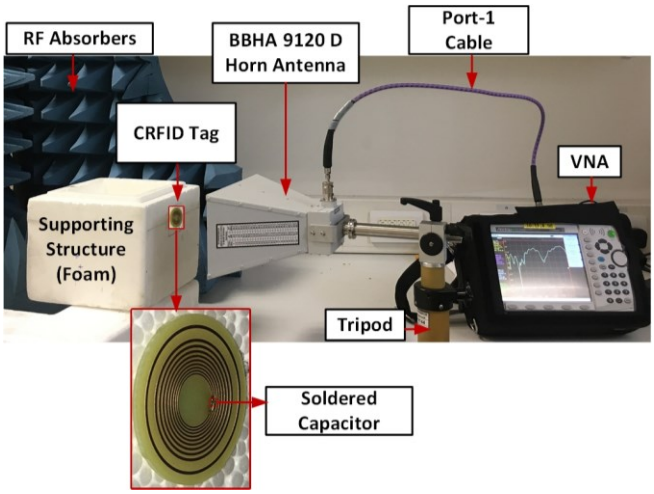


Fig. 7. Measurement setup for RCS calculations.

To calculate the RCS, one port reflection coefficient (S_{11}) measurement is first undertaken in isolation (To get the one port reflection coefficient of the horn antenna) with all the structures in place without the tag ($S_{11_{Iso}}$). The second measurement of a flat copper plate (25 mm x 25 mm) as a calibration object ($S_{11_{Ref}}$) is recorded on the VNA ($S_{11_{Ref}}$). In our case, it is found that using a flat metal plate with dimensions close to the tag under the test provided better RCS measurement. Third, the tag under test is placed, and a measurement is taken ($S_{11_{Tag}}$). The first and second calibration steps mentioned above are required only once and can be used to test multiple tags, given that the test bench and environment around it remain unchanged. The known RCS (of the flat metal plate (σ_{Ref}) is calculated using Equation (3).

$$\text{RCS}\ (\sigma_{Ref}) = 4\pi\frac{A^2}{\lambda^2}\ \text{m}^2 \qquad (3)$$

(where A=area, $\pi = 3.14$, and λ is the wavelength)

B. Results

The measured RCS results are compared with simulated results for verification. The RCS is measured to validate the encoding information. In Fig.8a, the simulation and measurement results are compared for Tag-1. Good agreement between simulated and measured results are achieved with a small (Less than 50 MHz) shift in the minima locations for 8-bit encoding. It is observed that the results for Tag-2 (Fig.8b) and Tag-3 (Fig.8c) compared well with simulation results. A discrepancy of less than 50 MHz is observed for Tag-2 and Tag-3, except ~100 MHz shift of b_{C4} minima in tag-3, which could be due to fabrication and measurement process. The measured results are smoothened using a moving average with period eight in Microsoft excel software.

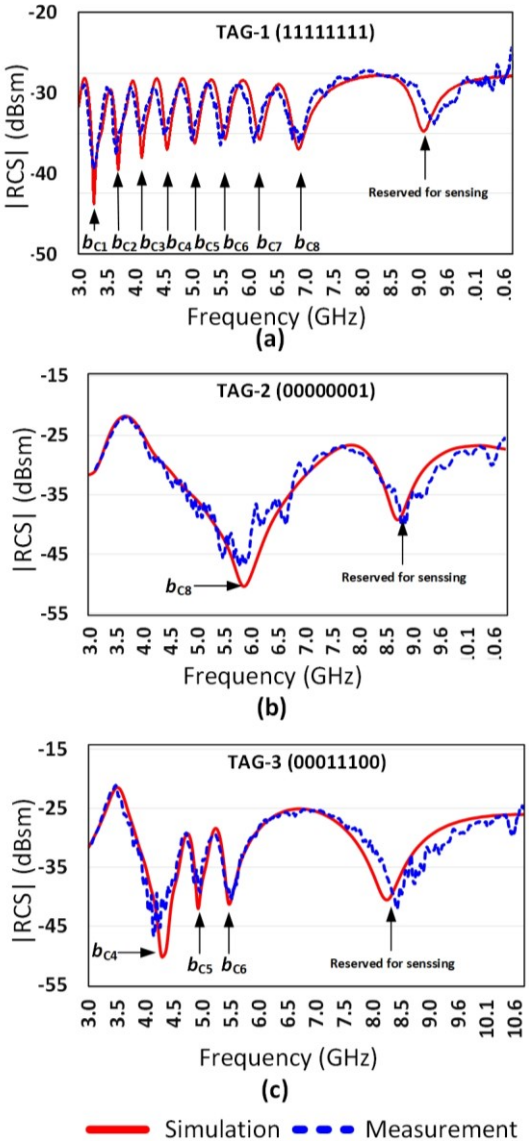


Fig. 8. Simulated vs Measured results for (a) Tag-1, (b) Tag-2, and (c) Tag-3.

IV. Comparison to the State of the Art

The proposed tag is compared with the state of the art nested CRR based CRFID tag designs found in the literature (Table II). It shows that the CRFID tag proposed in this paper provides a reliable encoding technique with a monostatic measurement setup.

TABLE II. Comparison with state-of-the-art CRR based CRFID tags.

Ref.	Bits	Size (mm)	Read Range (mm)	Single Layer?	RCS Meas.
[25]	1	45*45	NA	Yes	BM
[14]	19	30*30	400	No	BM
This work	8	Φ = 25	160	Yes	MM

Φ = Diameter of the tag; mm = Millimeter; BM = Bi-static Measurements (Two horn antennas); MM = Monostatic Measurement (Using single linearly polarized antenna)

V. CONCLUSION AND FUTURE WORK

An 8-bit CRFID tag with calibration ring principle and reserved sensing bit is discussed in this paper. A novel design principle is shown using a calibration ring, which reduces the errors in decoding the bit information in the RCS response. The encoding uses the presence of minima to represent bit '1' and their absence for bit '0'. The tag is a single layer RCS based CRFID tag. A monostatic measurement using one linearly polarized antenna provides accurate results for decoding encoded information. It proves that this method provides accurate measurable RCS data for three different tags. This tag design can then be used for accurate identification. Future work will investigate integrating and testing the tag within a contact lens for an animal health monitoring application. Further, the tag will be optimized to work on a lossy medium (such as an eye). Additionally, the aim is to test the sensing bit and its working principle to add sensing capability to the tag. Future work will also involve optimizing the read range and improving the data encoding capacity.

ACKNOWLEDGMENT

This paper has emanated from research funding provided by Science Foundation Ireland (SFI) as part of the SFI Centre VistaMilk (SFI 16/RC/3835). Aspects of this work have been supported under the following Grant Numbers: Connect Centre for Future Networks and Communications (13/RC/2077), The Insight Centre for Data Analytics (SFI/12/RC/2289) as well as the Enterprise Ireland funded Holistics DTIF (EI-DT20180291-A). All work is co-funded under the European Regional Development Fund.

REFERENCES

[1] S. Preradovic and N. C. Karmakar, "Chipless RFID: Bar code of the future," *IEEE microwave magazine,* vol. 11, no. 7, pp. 87-97, 2010.

[2] N. C. Karmaker, "Tag, you're it radar cross section of chipless RFID tags," *IEEE Microwave Magazine,* vol. 17, no. 7, pp. 64-74, 2016.

[3] D. R. Gawade *et al.*, "A battery-less NFC sensor transponder for museum artefact monitoring-a review of NFC sensor technology and a proposed solution," 2019.

[4] E. Perret, *Radio Frequency Identification and Sensors: From RFID to Chipless RFID*. John Wiley & Sons, 2014.

[5] D. R. Gawade *et al.*, "A Smart Archive Box for Museum Artifact Monitoring Using Battery-Less Temperature and Humidity Sensing," *Sensors,* vol. 21, no. 14, p. 4903, 2021.

[6] C. Herrojo, F. Paredes, J. Mata-Contreras, and F. Martín, "Chipless-RFID: A review and recent developments," *Sensors,* vol. 19, no. 15, p. 3385, 2019.

[7] Z. Abbasi, P. Shariaty, Z. Hashisho, and M. Daneshmand, "SilicaGel-Integrated Chipless RF Tag for Humidity Sensing," in *2018 18th International Symposium on Antenna Technology and Applied Electromagnetics (ANTEM)*, 2018, pp. 1-2: IEEE.

[8] D. Betancourt, M. Barahona, K. Haase, G. Schmidt, A. Hübler, and F. Ellinger, "Design of printed chipless-RFID tags with QR-code appearance based on genetic algorithm," *IEEE Transactions on Antennas and Propagation,* vol. 65, no. 5, pp. 2190-2195, 2017.

[9] A. Lazaro *et al.*, "Chipless dielectric constant sensor for structural health testing," *IEEE Sensors Journal,* vol. 18, no. 13, pp. 5576-5585, 2018.

[10] A. M. J. Marindra and G. Y. Tian, "Chipless RFID sensor tag for metal crack detection and characterization," *IEEE Transactions on Microwave Theory and Techniques,* vol. 66, no. 5, pp. 2452-2462, 2018.

[11] V. Sharma, S. Malhotra, and M. Hashmi, "Slot resonator based novel orientation independent chipless RFID tag configurations," *IEEE Sensors Journal,* vol. 19, no. 13, pp. 5153-5160, 2019.

[12] A. Vena, E. Perret, and S. Tedjini, "A fully printable chipless RFID tag with detuning correction technique," *IEEE Microwave and Wireless Components Letters,* vol. 22, no. 4, pp. 209-211, 2012.

[13] A. Vena, E. Perret, and S. Tedjini, "Design of compact and auto-compensated single-layer chipless RFID tag," *IEEE Transactions on Microwave Theory and Techniques,* vol. 60, no. 9, pp. 2913-2924, 2012.

[14] A. Vena, E. Perret, and S. Tedjini, "High-capacity chipless RFID tag insensitive to the polarization," *IEEE Transactions on Antennas and Propagation,* vol. 60, no. 10, pp. 4509-4515, 2012.

[15] A. Vena, E. Perret, S. Tedjini, D. Kaddour, A. Potie, and T. Barron, "A compact chipless RFID tag with environment sensing capability," in *2012 IEEE/MTT-S International Microwave Symposium Digest*, 2012, pp. 1-3: IEEE.

[16] C. A. Balanis, *Antenna theory: analysis and design*. John wiley & sons, 2016.

[17] S. Fan, T. Chang, X. Liu, Y. Fan, and M. M. Tentzeris, "A depolarizing chipless RFID tag with humidity sensing capability," in *2018 IEEE International Symposium on Antennas and Propagation & USNC/URSI National Radio Science Meeting*, 2018, pp. 2469-2470: IEEE.

[18] A. Guillet, A. Vena, E. Perret, and S. Tedjini, "Design of a chipless RFID sensor for water level detection," in *2012 15 International Symposium on Antenna Technology and Applied Electromagnetics*, 2012, pp. 1-4: IEEE.

[19] E. F. Knott, J. F. Schaeffer, and M. T. Tulley, *Radar cross section*. SciTech Publishing, 2004.

[20] M. Garbati, E. Perret, R. Siragusa, and C. Halope, "Ultrawideband chipless RFID: Reader technology from SFCW to IR-UWB," *IEEE Microwave Magazine,* vol. 20, no. 6, pp. 74-88, 2019.

[21] W. Chew, "A broad-band annular-ring microstrip antenna," *IEEE Transactions on Antennas and Propagation,* vol. 30, no. 5, pp. 918-922, 1982.

[22] CST. (2021). *CST Studio suite electromagnetic field simulation software*. Available: https://www.3ds.com/products-services/simulia/products/cst-studio-suite/

[23] W. Wiesbeck and D. Kahny, "Single reference, three target calibration and error correction for monostatic, polarimetric free space measurements," *Proceedings of the IEEE,* vol. 79, no. 10, pp. 1551-1558, 1991.

[24] Anritsu. *Anritsu VNA Master and Spectrum Analyzer*. Available: https://www.anritsu.com/en-us/test-measurement/products/ms2038c

[25] F. Villa-Gonzalez, R. Bhattacharyya, and S. Sarma, "Single and bulk identification of plastics in the recycling chain using Chipless RFID tags," in *2021 IEEE International Conference on RFID (RFID)*, 2021, pp. 1-8: IEEE.